Progress In Electromagnetics Research M, Vol. 22, 13–25, 2012

FDTD STUDY ON SCATTERING FOR CONDUCTING TARGET COATED WITH MAGNETIZED PLASMA OF TIME-VARYING PARABOLIC DENSITY DISTRIBUTION

S. Liu* **and S. Zhong**

School of Sciences, Nanchang University, Jiangxi 330031, China

Abstract—The trapezoidal recursive convolution (TRC) finite-difference time-domain (FDTD) method is extended to study the bistatic scattering radar cross sections (RCS) of conductive targets covered with inhomogeneous, time-varying, magnetized plasma medium. The two-dimensional TRC-FDTD formulations for electromagnetic scattering of magnetized plasma are derived. Time-varying parabolic density profiles of plasma are assumed in this paper. The bistatic radar cross sections are calculated under different conditions using 2-D TE model for a conductive cylinder covered with magnetized plasma. The numerical results show that plasma cloaking system can successfully reduce the bistatic RCS, that the plasma stealth is effective, and that the appropriate parameters of plasma can enhance its effectiveness.

1. INTRODUCTION

The finite-difference time-domain method has been widely used in solving many electromagnetic problems including those concerned with plasma media [1–8]. There has been considerable interest in the scattering of electromagnetic wave from conductive target covered with plasma, because it can be applied in plasma stealth technology. It is well known that plasma can attenuate the energy of incident ME wave. Much work concerning the scattering of the electromagnetic (EM) wave by conductive target covered with plasma have been discussed [9–11]. Recently frequency shifting of an EM wave in time–varying plasma has been extensively studied and the reflections

Received 31 August 2011, Accepted 10 November 2011, Scheduled 15 November 2011

* Corresponding author: Song Liu (sliu@ncu.edu.cn).

of the conductive target covered with inhomogeneous plasma were calculated [12–14]. For there is an externally applied magnetic field cases, the plasma exhibits anisotropic behavior and its permittivity takes a tensor form. Wave propagation and scattering in an anisotropic medium are nonreciprocal and the implementation of the conventional FDTD method is difficult [15]. Over the last decade, the FDTD and various algorithms have been extended to simulate anisotropic media [16–20].

In this paper, the TRC-FDTD approach is extended to study the bistatic RCS of conductive targets covered with inhomogeneous magnetized plasma medium. Parabolic and Time-varying parabolic density profiles of plasma are assumed in this paper. The two-dimensional TRC-FDTD formulations for electromagnetic scattering of magnetized plasma are derived. The bistatic radar cross sections are calculated under different conditions using 2-D TE model for a conductive cylinder covered with inhomogeneous, time-varying magnetized plasma. The numerical results illustrate that plasma cloaking target can successfully reduce the bistatic RCS, the plasma stealth is effective, and the proper parameters of plasma can enhance its effectiveness.

2. TRC-FDTD FORMULATIONS IN MAGNETIZED PLASMA MEDIUM

The Maxwell's curl equations in magnetized plasma are given by

$$\frac{\partial \mathbf{D}}{\partial t} = \nabla \times \mathbf{H}, \tag{1}$$

$$\frac{\partial \mathbf{H}}{\partial t} = -\frac{1}{\mu_0} \nabla \times \mathbf{E}. \tag{2}$$

Considering the external static magnetic field is parallel to the z axis. The tensor permittivity expression for the magnetized plasmas is

$$\tilde{\boldsymbol{\varepsilon}}_{ij}(\omega) = \begin{vmatrix} \varepsilon_{xx}(\omega) & j\varepsilon_{xy}(\omega) & 0 \\ -j\varepsilon_{yx}(\omega) & \varepsilon_{yy}(\omega) & 0 \\ 0 & 0 & \varepsilon_{zz}(\omega) \end{vmatrix}, \tag{3}$$

where the components of this tensor are

$$\varepsilon_{xx}(\omega) = \varepsilon_{yy}(\omega) = \varepsilon_0 \left(1 - \frac{\left(\frac{\omega_p}{\omega}\right)^2 \left(1 - j\frac{\nu}{\omega}\right)}{\left(1 - j\frac{\nu}{\omega}\right)^2 - \left(\frac{\omega_b}{\omega}\right)^2} \right), \tag{4}$$

$$\varepsilon_{zz}(\omega) = \varepsilon_0 \left(1 - \frac{\omega_p^2}{\omega(\omega - j\nu)} \right), \tag{5}$$

$$\varepsilon_{xy}(\omega) = \varepsilon_{yx}(\omega) = \varepsilon_0 \frac{\left(\frac{\omega_p}{\omega}\right)^2 \left(\frac{\omega_b}{\omega}\right)}{\left(1 - j\frac{\nu}{\omega}\right)^2 - \left(\frac{\omega_b}{\omega}\right)^2}, \tag{6}$$

where $j = \sqrt{-1}$, ε_0 is the permittivity of free space, ν is the electron collision frequency, $\omega_p = \sqrt{n_e e^2/m\varepsilon_0}$ is the plasma frequency, n_e is the electron number density, $\omega_b = eB_0/m$ is the electron cyclotron frequency, B_0 is the external magnetic field. e and m are the electric charge and mass of an electron, respectively.

The relationship between the electric field and the electric flux density is

$$\mathbf{D}_i(\omega) = \tilde{\boldsymbol{\varepsilon}}_{ij}(\omega) \cdot \mathbf{E}_j(\omega), \tag{7}$$

In the time domain, by use of the convolution integral, we have

$$D_x(t) = \varepsilon_0 E_x(t) + \varepsilon_0 \int_0^t E_x(t-\tau)\chi_{xx}(\tau)d\tau - \varepsilon_0 \int_0^t E_y(t-\tau)\chi_{xy}(\tau)d\tau, \tag{8}$$

$$D_y(t) = \varepsilon_0 E_y(t) + \varepsilon_0 \int_0^t E_y(t-\tau)\chi_{yy}(\tau)d\tau + \varepsilon_0 \int_0^t E_x(t-\tau)\chi_{yx}(\tau)d\tau, \tag{9}$$

where t is the time.

The time-domain susceptibility functions has been obtained from the frequency-domain permittivity functions by inverse Fourier transformation, and are shown as follow

$$\begin{aligned}\chi_{xx}(\tau) &= \chi_{yy}(\tau) \\ &= \frac{\omega_p^2}{\nu^2+\omega_b^2}\{\nu - \exp(-\nu\tau)[\nu\cos(\omega_b\tau) - \omega_b\sin(\omega_b\tau)]\}U(\tau),\end{aligned} \tag{10}$$

$$\begin{aligned}\chi_{xy}(\tau) &= \chi_{yx}(\tau) \\ &= \frac{\omega_p^2}{\nu^2+\omega_b^2}\{\omega_b - \exp(-\nu\tau)[\omega_b\cos(\omega_b\tau) + \nu\sin(\omega_b\tau)]\}U(\tau),\end{aligned} \tag{11}$$

where $U(\tau)$ is the unit step function.

The evaluation of (10) and (11) will be simplified if we introduce a complex susceptibility function and simply take its real part when computing the convolution. The complex susceptibilities can be given by

$$\tilde{\chi}_{xx}(\tau) = \tilde{\chi}_{yy}(\tau) = \frac{\omega_p^2}{\nu^2+\omega_b^2}(\nu + j\omega_b)\{1 - \exp[-(\nu - j\omega_b)\tau]\}U(\tau), \tag{12}$$

$$\tilde{\chi}_{xy}(\tau) = \tilde{\chi}_{yx}(\tau) = \frac{\omega_p^2}{\nu^2+\omega_b^2}(\omega_b - j\nu)\{1 - \exp[-(\nu - j\omega_b)\tau]\}U(\tau), \tag{13}$$

with

$$\chi_{xx}(\tau) = \chi_{yy}(\tau) = \mathrm{Re}[\tilde{\chi}_{xx}(\tau)] = \mathrm{Re}[\tilde{\chi}_{yy}(\tau)], \tag{14}$$

$$\chi_{xy}(\tau) = \chi_{yx}(\tau) = \mathrm{Re}[\tilde{\chi}_{xy}(\tau)] = \mathrm{Re}[\tilde{\chi}_{yx}(\tau)], \tag{15}$$

Using Yee's notation, we let $t = n\Delta t$ in (8)–(9), the each component of $\mathbf{D}$ can be written as

$$\begin{aligned}\tilde{D}_x^n = {} & \varepsilon_0 E_x^n + \varepsilon_0 \int_0^{n\Delta t} E_x(n\Delta t - \tau)\tilde{\chi}_{xx}(\tau)d\tau \\ & - \varepsilon_0 \int_0^{n\Delta t} E_y(n\Delta t - \tau)\tilde{\chi}_{xy}(\tau)d\tau,\end{aligned} \tag{16}$$

$$\begin{aligned}\tilde{D}_y^n = {} & \varepsilon_0 E_y^n + \varepsilon_0 \int_0^{n\Delta t} E_y(n\Delta t - \tau)\tilde{\chi}_{yy}(\tau)d\tau \\ & + \varepsilon_0 \int_0^{n\Delta t} E_x(n\Delta t - \tau)\tilde{\chi}_{yx}(\tau)d\tau.\end{aligned} \tag{17}$$

Using TRC method [5], (16) is approximated using an average of the electric fields over two consecutive time steps in the following form

$$\frac{D_x^n}{\varepsilon_0} = E_x^n + \sum_{m=0}^{n-1}\left[\frac{E_x^{n-m} + E_x^{n-m-1}}{2}\chi_{xx}^m - \frac{E_y^{n-m} + E_y^{n-m-1}}{2}\chi_{yy}^m\right]. \tag{18}$$

Then, the D_x for $n+1$ time steps can be written as

$$\frac{D_x^{n+1}}{\varepsilon_0} = E_x^{n+1} + \sum_{m=0}^{n}\left[\frac{E_x^{n-m+1} + E_x^{n-m}}{2}\chi_{xx}^m - \frac{E_y^{n-m+1} + E_y^{n-m}}{2}\chi_{yy}^m\right], \tag{19}$$

where

$$\begin{aligned}\chi_{xx}^m &= \mathrm{Re}(\tilde{\chi}_{xx}^m) = \mathrm{Re}\left[\int_{m\Delta t}^{(m+1)\Delta t} \tilde{\chi}_{xx}(\tau)d\tau\right] \\ &= \mathrm{Re}\left[\int_{m\Delta t}^{(m+1)\Delta t} \tilde{\chi}_{yy}(\tau)d\tau\right],\end{aligned} \tag{20}$$

$$\begin{aligned}\chi_{xy}^m &= \mathrm{Re}(\tilde{\chi}_2^m) = \mathrm{Re}\left[\int_{m\Delta t}^{(m+1)\Delta t} \tilde{\chi}_{xy}(\tau)d\tau\right] \\ &= \mathrm{Re}\left[\int_{m\Delta t}^{(m+1)\Delta t} \tilde{\chi}_{yx}(\tau)d\tau\right].\end{aligned} \tag{21}$$

Substituting (12)–(13) in (20)–(21), we can acquire

$$\begin{aligned}\tilde{\chi}_{xx}^{m} &= \int_{m\Delta t}^{(m+1)\Delta t} \tilde{\chi}_{xx}(\tau)d\tau = \int_{m\Delta t}^{(m+1)\Delta t} \tilde{\chi}_{yy}(\tau)d\tau \\ &= \int_{m\Delta t}^{(m+1)\Delta t} \frac{\omega_p^2}{\nu^2+\omega_b^2}(\nu+j\omega_b)\left\{1-\exp\left[-(\nu-j\omega_b)\tau\right]\right\}U(\tau)d\tau \\ &= \frac{\omega_p^2(\nu+j\omega_b)}{\nu^2+\omega_b^2}\Delta t - \frac{\omega_p^2}{\nu^2+\omega_b^2}\frac{\nu+j\omega_b}{\nu-j\omega_b}\left\{1-\exp\left[-(\nu-j\omega_b)\Delta t\right]\right\} \\ &\quad \exp\left[-(\nu-j\omega_b)m\Delta t\right], \qquad (22)\end{aligned}$$

$$\begin{aligned}\tilde{\chi}_{xy}^{m} &= \int_{m\Delta t}^{(m+1)\Delta t} \tilde{\chi}_{xy}(\tau)d\tau = \int_{m\Delta t}^{(m+1)\Delta t} \tilde{\chi}_{yx}(\tau)d\tau \\ &= \int_{m\Delta t}^{(m+1)\Delta t} \frac{\omega_p^2}{\nu^2+\omega_b^2}(\omega_b-j\nu)\left\{1-\exp\left[-(\nu-j\omega_b)\tau\right]\right\}U(\tau)d\tau \\ &= \frac{\omega_p^2(\omega_b-j\nu)}{\nu^2+\omega_b^2}\Delta t - \frac{\omega_p^2}{\nu^2+\omega_p^2}\frac{(\omega_b-j\nu)}{(\nu-j\omega_b)}\left\{1-\exp\left[-(\nu-j\omega_b)\Delta t\right]\right\} \\ &\quad \exp\left[-(\nu-j\omega_b)m\Delta t\right]. \qquad (23)\end{aligned}$$

Letting

$$\Delta\chi_{xx}^{m} = \mathrm{Re}(\Delta\tilde{\chi}_{xx}^{m}) = \mathrm{Re}\left(\tilde{\chi}_{xx}^{m}-\tilde{\chi}_{xx}^{m+1}\right) = \chi_{xx}^{m}-\chi_{xx}^{m+1}, \qquad (24)$$

$$\Delta\chi_{xy}^{m} = \mathrm{Re}(\Delta\tilde{\chi}_{xy}^{m}) = \mathrm{Re}\left(\tilde{\chi}_{xy}^{m}-\tilde{\chi}_{xy}^{m+1}\right) = \chi_{xy}^{m}-\chi_{xy}^{m+1}. \qquad (25)$$

From (18) and (19), we obtain

$$\begin{aligned}\frac{D_x^{n+1}-D_x^{n}}{\varepsilon_0} &= \left(1+\frac{\chi_{xx}^{0}}{2}\right)E_x^{n+1} - \left(1-\frac{\chi_{xx}^{0}}{2}\right)E_x^{n} - \left(\frac{\chi_{xy}^{0}}{2}\right)E_y^{n+1} \\ &\quad - \left(\frac{\chi_{xy}^{0}}{2}\right)E_y^{n} - \psi_{xx}^{n} + \psi_{yxy}^{n}, \qquad (26)\end{aligned}$$

Equation (1) is discretized using the Yee grid and leap-frog integration

$$\frac{D_x^{n+1}-D_x^{n}}{\Delta t} = (\nabla\times\mathbf{H})_x^{n+1/2}, \qquad (27)$$

In views of (26) and (27), we find

$$\begin{aligned}\left(1+\frac{\chi_{xx}^{0}}{2}\right)E_x^{n+1} &= \left(1-\frac{\chi_{xx}^{0}}{2}\right)E_x^{n} + \frac{\chi_{xy}^{0}}{2}E_y^{n+1} + \frac{\chi_{xy}^{0}}{2}E_y^{n} + \psi_{xx}^{n} \\ &\quad -\psi_{yxy}^{n} + \frac{\Delta t}{\varepsilon_0}\left(\nabla\times\mathbf{H}\right)_x^{n+1/2}. \qquad (28)\end{aligned}$$

where

$$\chi^0_{xx} = \mathrm{Re}\left(\tilde{\chi}^0_{xx}\right), \quad \chi^0_{xy} = \mathrm{Re}\left(\tilde{\chi}^0_{xy}\right),$$
$$\psi^n_{xx} = \sum_{m=0}^{n-1} \frac{\left(E_x^{n-m} + E_x^{n-m-1}\right)}{2} \Delta\chi^m_{xx},$$
$$\psi_{yxy} = \sum_{m=0}^{n-1} \frac{\left(E_y^{n-m} + E_y^{n-m-1}\right)}{2} \Delta\chi^m_{xy}.$$

By the same procedure

$$\left(1 + \frac{\chi^0_{yy}}{2}\right) E_y^{n+1} = \left(1 - \frac{\chi^0_{yy}}{2}\right) E_y^n - \frac{\chi^0_{yx}}{2} E_x^{n+1} - \frac{\chi^0_{yx}}{2} E_x^n + \psi^n_{yy} + \psi^n_{xyx} + \frac{\Delta t}{\varepsilon_0} (\nabla \times \mathbf{H})_y^{n+1/2}, \tag{29}$$

where

$$\chi^0_{yy} = \chi^0_{xx}, \quad \chi^0_{yx} = \chi^0_{xy}, \quad \psi^n_{yy} = \sum_{m=0}^{n-1} \frac{\left(E_y^{n-m} + E_y^{n-m-1}\right)}{2} \Delta\chi^m_{yy},$$
$$\psi^n_{xyx} = \sum_{m=0}^{n-1} \frac{\left(E_x^{n-m} + E_x^{n-m-1}\right)}{2} \Delta\chi^m_{yx}.$$

The TRC-FDTD updated equations for two-dimensional TE case are derived

$$E_x^{n+1} = \frac{\left(1 - \left(\frac{\chi^0_{xx}}{2}\right)^2\right) - \left(\frac{\chi^0_{xy}}{2}\right)^2}{\left(1 + \frac{\chi^0_{xx}}{2}\right)^2 + \left(\frac{\chi^0_{xy}}{2}\right)^2} E_x^n + \frac{\chi^0_{xy}}{\left(1 + \frac{\chi^0_{xx}}{2}\right)^2 + \left(\frac{\chi^0_{xy}}{2}\right)^2} E_y^n$$
$$+ \frac{\frac{\chi^0_{xy}}{2}}{\left(1 + \frac{\chi^0_{xx}}{2}\right)^2 + \left(\frac{\chi^0_{xy}}{2}\right)^2} \cdot (\psi^n_{yy} + \psi^n_{xyx}) + \frac{1 + \frac{\chi^0_{xx}}{2}}{\left(1 + \frac{\chi^0_{xx}}{2}\right)^2 + \left(\frac{\chi^0_{xy}}{2}\right)^2} (\psi^n_{xx} - \psi^n_{yxy})$$
$$+ \frac{\frac{\chi^0_{xy}}{2}}{\left(1 + \frac{\chi^0_{xx}}{2}\right)^2 + \left(\frac{\chi^0_{xy}}{2}\right)^2} \left(\frac{\Delta t}{\varepsilon_0} (\nabla \times \mathbf{H})_y^{n+1/2}\right)$$
$$+ \frac{1 + \frac{\chi^0_{xx}}{2}}{\left(1 + \frac{\chi^0_{xx}}{2}\right)^2 + \left(\frac{\chi^0_{xy}}{2}\right)^2} \left(\frac{\Delta t}{\varepsilon_0} (\nabla \times \mathbf{H})_x^{n+1/2}\right), \tag{30}$$

$$E_y^{n+1} = \frac{\left(1-\left(\frac{\chi_{xx}^0}{2}\right)^2\right)-\left(\frac{\chi_{xy}^0}{2}\right)^2}{\left(1+\frac{\chi_{xx}^0}{2}\right)^2+\left(\frac{\chi_{xy}^0}{2}\right)^2}E_y^n - \frac{\chi_{xy}^0}{\left(1+\frac{\chi_{xx}^0}{2}\right)^2+\left(\frac{\chi_{xy}^0}{2}\right)^2}E_x^n$$
$$-\frac{\frac{\chi_{xy}^0}{2}}{\left(1+\frac{\chi_{xx}^0}{2}\right)^2+\left(\frac{\chi_{xy}^0}{2}\right)^2}\cdot(\psi_{xx}^n-\psi_{yxy}^n)+\frac{1+\frac{\chi_{xx}^0}{2}}{\left(1+\frac{\chi_{xx}^0}{2}\right)^2+\left(\frac{\chi_{xy}^0}{2}\right)^2}(\psi_{yy}^n+\psi_{xyx}^n)$$
$$-\frac{\frac{\chi_{xy}^0}{2}}{\left(1+\frac{\chi_{xx}^0}{2}\right)^2+\left(\frac{\chi_{xy}^0}{2}\right)^2}\left(\frac{\Delta t}{\varepsilon_0}(\nabla\times\mathbf{H})_x^{n+1/2}\right)$$
$$+\frac{1+\frac{\chi_{xx}^0}{2}}{\left(1+\frac{\chi_{xx}^0}{2}\right)^2+\left(\frac{\chi_{xy}^0}{2}\right)^2}\left(\frac{\Delta t}{\varepsilon_0}(\nabla\times\mathbf{H})_y^{n+1/2}\right), \tag{31}$$

where

$$\begin{aligned}\psi_{xx}^n &= \mathrm{Re}\left(\tilde{\psi}_{xx}^n\right)\\ &= \mathrm{Re}\left(\frac{\Delta\chi_{xx}^0}{2}E_x^n+\frac{\Delta\chi_{xx}^0}{2}E_x^{n-1}+\exp\left[-(\nu-j\omega_b)\Delta t\right]\tilde{\psi}_{xx}^{n-1}\right),\\ \psi_{yxy}^n &= \mathrm{Re}(\tilde{\psi}_{xy}^n)\\ &= \mathrm{Re}\left(\frac{\Delta\chi_{xy}^0}{2}E_y^n+\frac{\Delta\chi_{xy}^0}{2}E_y^{n-1}+\exp\left[-(\nu-j\omega_b)\Delta t\right]\tilde{\psi}_{yxy}^{n-1}\right),\\ \psi_{yy}^n &= \mathrm{Re}(\tilde{\psi}_{yy}^n)\\ &= \mathrm{Re}\left(\frac{\Delta\chi_{yy}^0}{2}E_y^n+\frac{\Delta\chi_{yy}^0}{2}E_y^{n-1}+\exp\left[-(\nu-j\omega_b)\Delta t\right]\tilde{\psi}_{yy}^{n-1}\right),\\ \psi_{xyx}^n &= \mathrm{Re}(\tilde{\psi}_{yx}^n)\\ &= \mathrm{Re}\left(\frac{\Delta\chi_{yx}^0}{2}E_x^n+\frac{\Delta\chi_{yx}^0}{2}E_x^{n-1}+\exp\left[-(\nu-j\omega_b)\Delta t\right]\tilde{\psi}_{xyx}^{n-1}\right).\end{aligned}$$

The H_z component is updated as traditional FDTD. In addition, in the iterative equations, when one field value is dispersed at one space point and other fields are not located at the point, these values are not available directly from the Yee's FDTD cell. Instead, they must be interpolated from neighboring quantities. Therefore, the following

average approximations are used, i.e.,

$$E_y^n\left(i+\frac{1}{2},j\right)=\frac{1}{4}\left[E_y^n\left(i,j+\frac{1}{2}\right)+E_y^n\left(i,j-\frac{1}{2}\right)\right.$$
$$\left.+E_y^n\left(i+1,j+\frac{1}{2}\right)+E_y^n\left(i+1,j-\frac{1}{2}\right)\right], \quad (32)$$

$$\psi_{yy}^n\left(i+\frac{1}{2},j\right)=\frac{1}{4}\left[\psi_{yy}^n\left(i,j+\frac{1}{2}\right)+\psi_{yy}^n\left(i,j-\frac{1}{2}\right)\right.$$
$$\left.+\psi_{yy}^n\left(i+1,j+\frac{1}{2}\right)+\psi_{yy}^n\left(i+1,j-\frac{1}{2}\right)\right]. \quad (33)$$

Similar expressions can be obtained for other field components.

3. THE BISTATIC RCS OF CONDUCTING CYLINDER COVERED WITH MAGNETIZED PLASMA

In this section, we will provide some numerical solutions to the problem of electromagnetic scattering by an infinitely long perfectly conducting cylinder covered with inhomogeneous time-varying, collision, cold, magnetized plasma. The radius of cylinder is $a = 0.15\,\mathrm{m}$, its axis is along $\hat{z}$ axis. The external biasing magnetic field is parallel to $\hat{z}$ axis. The Parabolic and Time-varying parabolic density profiles of plasma are assumed in this paper. The incident plane wave of frequency $f = 1\,\mathrm{GHz}$ is assumed to have an electric field amplitude equal to unity, to propagate in the $+\hat{x}$ direction and to be polarized in parallel to $\hat{y}$ axis. The FDTD parameters: the size of space step $\delta = 0.015\,\mathrm{m}$. The time step $\Delta t = 0.5\delta/c$, where c is the speed of light in vacuum. The computational domain is subdivided into $80 \times 80\delta^2$. Five cells PML absorbing boundaries were used at the terminations of the space to eliminate unwanted reflections [21]. The simulations were allowed to run for 1100 time steps.

The plasma electron density derived in the laboratory distributes as parabolic density profile. The plasma frequency is given by

$$\omega_p(r)=\omega_{p1}+\omega_{p2}\frac{r}{d}, \quad (34)$$

where r is the vertical distance between any point in plasma and the surface of the conductive target, d is the thickness of the plasma coating.

The plasma electron density derived in the laboratory distributes as Time-varying parabolic density profile. The plasma frequency is given by

$$\omega_p(r,t)=\left(\omega_{p1}+\omega_{p2}\frac{r}{d}\right)\frac{t}{T_r} \quad (35)$$

where $\omega_{p1} = 3.14\times10^9$ rad/s, $\omega_{p2} = 20\pi\times10^9$ rad/s, T_r is the relaxation time of plasma.

3.1. Effects of Plasma Thickness on RCS

In this subsection, the relationships between RCS and bistatic angle with the plasma thickness varying are discussed. Fig. 1 plots RCS of the conductive cylinder covered by plasma with a parabolic density profile versus bistatic angle, where the plasma collision frequency $v = 6$ GHz, and the electron cyclotron frequency $\omega_b = 3$ Grad/s, among them the RCS ($d = 0$) without plasma cloaking is also plotted for comparison. It is clear from Fig. 1 that a plasma cloaking system can successfully reduce RCS, and these curves of RCS become bilateral unsymmetry in the scattering angle interval of 0° to 360°. This is mainly due to the fact that the two components of electric field are coupled on account of the external magnetic field. We also can see from these plots that the RCS decreases with an increasing thickness of plasma in the most scope of bistatic angle. However, in the range of $30° \sim 90°$, and $285° \sim 330°$, the RCS obviously increase with the increase of thickness of plasma. The simulation results demonstrate that an appropriate plasma thickness may efficiently reduce the RCS of the conducting cylinder coating plasma.

3.2. Effects of Electron Cyclotron Frequency on RCS

We fix the plasma thickness $d = 0.15$ m, let $\omega_b = 3$ Grad/s and $\omega_b = 9$ Grad/s, respectively, other parameters are the same as above. The RCS of the conductive cylinder covered by plasma with a parabolic density profile versus bistatic angle are given in Fig. 2.

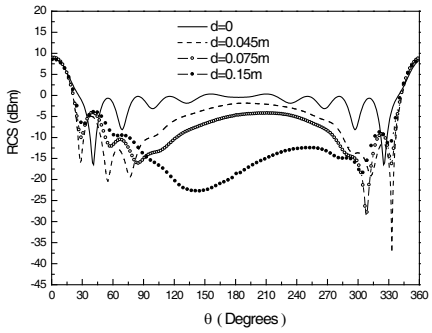

Figure 1. RCS versus bistatic angle in different plasma coating thickness.

From Fig. 2, it is also observed that these curves of the RCS are no longer bilateral symmetry in the area of scattering angles from 0° to 360°. Most of RCS obviously increases with the increase of the electron cyclotron frequency, whereas, the partial RCS decrease with the increase of the electron cyclotron frequency in interval of $315° \sim 340°$. The reason mainly is that the larger external magnetic field is, the stronger the coupling between the components of the electric field correspondingly, and the polarization directions of the electric field have been changed in plasma too.

3.3. Effects of Relaxation Time on RCS

The plasma thickness $d = 0.075$ m, the electron cyclotron frequency is 3 Grad/s, the relaxation time are 200, 500, and 1000 time steps, respectively. Other parameters are the same as above. Fig. 3 plots RCS of the conductive cylinder covered by plasma with a Time-varying parabolic density profile versus bistatic angle.

The testing results show that the longer relaxation time is, the larger the RCS at the fixed the plasma thickness and the electron cyclotron frequency, as shown in Fig. 3. In general, when the frequency of the incident electromagnetic wave is given, the longer relaxation time must prolong the arrival time of the maximum density of plasma layer. The bigger the plasma electron density is, the more the numbers of polarized electron, which implies that the plasma layer has a stronger absorbing ability.

For the conductive cylinder, the above results indicate that the plasma cloaking layer can efficiently reduce the RCS in the backscattering ($\theta = 180°$) and small bistatic angle range. Nevertheless,

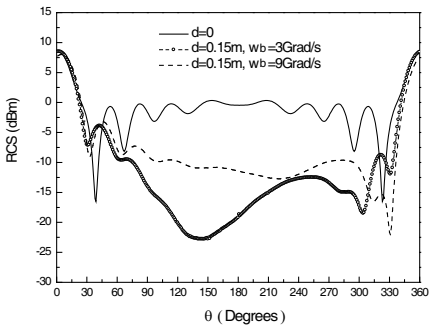

Figure 2. RCS versus bistatic angle in different the electron cyclotron frequency.

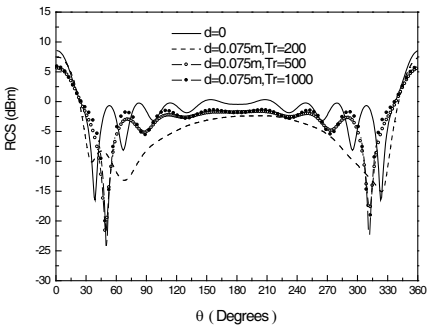

Figure 3. RCS versus bistatic angle in different relaxation time.

the RCS not only did not decrease and instead it slightly increase in the forward scattering ($\theta = 0°$) and large bistatic angle range. In fact, the plasma cloaking layer can enlarge the projecting area of conductive cylinder. The RCS of the forward scattering is approximately proportional to the projecting area of the target.

4. CONCLUSION

In this paper, the TRC-FDTD is applied to anisotropic magnetized plasma media. 2-D TRC-FDTD formulations for electromagnetic scattering of magnetized plasma are derived. Parabolic and Time-varying parabolic density profiles of plasma are assumed in this paper. The bistatic radar cross sections are calculated under different conditions using 2-D TE model for a conductive cylinder covered with magnetized plasma medium. The numerical results illustrate that the conductive cylinder cloaking plasma can successfully reduce the bistatic RCS, the plasma stealth is effective, and the proper parameters of plasma can enhance its effectiveness. It is also shown that the RCS of the conductive cylinder covered with plasma cloaking depends on many factors such as the electron density distributes profile of plasma, plasma thickness, and the relaxation time of time-varying plasma, etc. The studies can help us use the proper plasma distribution and have a significant application in aircraft stealthy technology.

ACKNOWLEDGMENT

The work is partially supported by the Natural Science Foundation of China under Grant number 11165011 and the Natural Science Foundation of Jiangxi Province under Grant number 2009GZW0016.

REFERENCES

1. Taflove, A. and C. H. Susan, *Computational Electrodynamics: The Finite-difference Time-domain Method*, Boston, Artech House, 2005.
2. Schneider, J. and S. Hudson, "The finite-difference time-domain method applied to anisotropic material," *IEEE Transactions on Antennas and Propagation*, Vol. 41, No. 7, 994–999, 1993.
3. Hunsberger, F., R. Luebbers, and K. Kunz, "Finite-difference time-domain analysis of gyrotropic media. I. Magnetized plasma," *IEEE Transactions on Antennas and Propagation*, Vol. 40, No. 12, 1489–1495, 1992.

4. Kelley, D. F. and R. J. Luebbers, "Piecewise linear recursive convolution for dispersive media using FDTD," *IEEE Transactions on Antennas and Propagation*, Vol. 44, No. 6, 792–797, 1996.
5. Siushansian, R. and J. LoVetri, "A comparison of numerical techniques for modeling electromagnetic dispersive media," *IEEE Microw. Guided Wave Lett.*, Vol. 5, No. 12, 426–428, 1995.
6. Chen, Q., M. Katsurai, and P. H. Aoyagi, "An FDTD formulation for dispersive media using a current density," *IEEE Transactions on Antennas and Propagation*, Vol. 46, No. 11, 1739–1746. 1998.
7. Liu, S. B., N. C. Yuan, and J. J. Mo, "Piecewise linear current density recursive convolution FDTD implementation for anisotropic magnetized plasmas," *IEEE Microwave Wireless Components Letters*, Vol. 14, No. 5, 222–224, 2004.
8. Liu, S. and S. B. Liu, "Runge-kutta exponential time differencing FDTD method for anisotropic magnetized plasma," *IEEE Antennas and Wireless Propagation Letters*, Vol. 7, 306–309, 2008.
9. Xu, L. J. and N. C. Yuan, "JEC-FDTD for 2-D conducting cylinder coated by anisotropic magnetized plasma," *IEEE Microwave Wireless Components Letters*, Vol. 15, No. 12, 892–894, 2005.
10. Xu, L. J. and N. C. Yuan, "FDTD for formulations for scattering from 3-D anisotropic magnetized plasma objects," *IEEE Antennas and Wireless Propagation Letters*, Vol. 5, 335–338, 2006.
11. Yang, L. X., "3D FDTD implementation for scattering of electric anisotropic dispersive medium using recursive convolution method," *International Journal of Infrared and Millimeter Waves*, Vol. 28, 557–565, 2007.
12. Liu, S. B., J. J. Mo, and N. C. Yuan, "FDTD simulation of electromagnetic reflection of conductive plane covered with inhomogeneous time-varying plasma," *International Journal of Infrared and Millimeter Waves*, Vol. 23, No. 8, 1179–1191, 2002.
13. Liu, S. B., J. J. Mo, and N. C. Yuan, "FDTD analysis of electromagnetic reflection of conductive plane covered with magnetized inhomogeneous plasmas," *International Journal of Infrared and Millimeter Waves*, Vol. 23, No. 12, 1803–1815, 2002.
14. Dai, S. Y., C. M. Zhang, and Z. S. Wu, "Electromagnetic scattering of objects above ground using MRTD/FDTD hybrid method," *Journal of Electromagnetic Waves and Applications*, Vol. 32, No. 16, 2187–2196, 2009.
15. Lee, J. H. and D. K. Kalluri, "Three-dimensional FDTD simulation of electromagnetic wave transformation in a dynamic

inhomogeneous magnetized plasma," *IEEE Trans. on Antennas and Propagation*, Vol. 47, No. 7, 1146–1151, 1999.

16. Prokopidis, K. P., E. P. Kosmidou, and T. D. Tsiboukis, "An FDTD algorithm for wave propagation in dispersive media using higher-order schemes," *Journal of Electromagnetic Waves and Applications,* Vol. 18, No. 9, 1171–1194, 2004.
17. Wang, M. Y., J. Wu, J. Wu, Y. Yan, and H.-L. Li, "FDTD study on scattering of metallic column covered by double-negative metamaterial," *Journal of Electromagnetic Waves and Applications*, Vol. 21, No. 14, 1905–1914, 2007.
18. Werner, G. R. and J. R. Cary, "Stable FDTD algorithm for non-diagonal, anisotropic dielectrics," *Journal of Computational Physics*, Vol. 226, 1085–1101, 2007.
19. Lee, Y.-G., "Electric field discontinuity-considered effective-permittivities and integration-tensors for the three-dimensional finite-difference time-domain method," *Progress In Electromagnetics Research*, Vol. 118, 335–354, 2011.
20. Geng, Y. L., X. B. Wu, and L. W. Li, "Characterization of electromagnetic scattering by a plasma anisotropic spherical shell," *IEEE Antennas and Wireless Propagation Letters*, Vol. 3, 100–103, 2004.
21. Berenger, J. P., "A perfectly matched layer for the absorption of electromagnetic waves," *J. Comput. Phys.*, Vol. 114, No. 1, 185–200, 1994.